JOURNAL OF SOLID STATE CHEMISTRY **125,** 102–107 (1996)
ARTICLE NO. 0270

The Crystal Structure of $Ba_8Ta_6NiO_{24}$: Cation Ordering in Hexagonal Perovskites

A. M. Abakumov,*,† G. Van Tendeloo,* A. A. Scheglov,† R. V. Shpanchenko,† and E. V. Antipov†

*EMAT, University of Antwerp (RUCA), Groenenborgerlaan 171, B-2020 Antwerp, Belgium; and †Chemical Department, Moscow State University, 119899 Moscow, Russia

Received February 1, 1996; accepted May 13, 1996

The new complex perovskite-like oxide $Ba_8Ta_6NiO_{24}$ was synthesized and its crystal structure was studied using X-ray powder diffraction, electron diffraction, and high resolution electron microscopy. The $Ba_8Ta_6NiO_{24}$ structure is based on a 8H $(cchc)_2$ close-packed stacking of BaO_3 layers (space group $P6_3cm$, $a = 10.07458(6)$ Å, $c = 19.0122(2)$ Å.). The structural refinement gave the following values of reliability factors: $R_F = 0.028$, $R_P = 0.042$, $R_{wP} = 0.056$. The main feature of this structure is the existence of two different pairs of face-sharing octahedra. In the first pair one octahedron is occupied by Ta whereas the other one is empty. In the second pair one of the two octahedra is occupied by Ta and a cation vacancy and its neighbor is occupied by Ni, Ta, or a vacancy. This distribution of cations was completely confirmed by electron microscopy. The formation of a $Ba_8Ta_{6+0.4x}Ni_{1-x}O_{24}$ solid solution with a narrow homogeneity range with $(-0.2 \le x \le 0.2)$ was observed. © 1996 Academic Press, Inc.

1. INTRODUCTION

The cubic perovskite structure can be described as a close-packed stacking of AX_3 layers, alternating along the [111] axis of perovskite subcell. Alternative structures arise when some of the ''cubic'' (c) layers are shifted by (1/3, 2/3, 0) introducing ''hexagonal'' (h) layers. As a consequence of such a shift groups of face-shared octahedra (FSO) appear. The separation between cations in neighboring FSO octahedra should approximately correspond to the average thickness of close-packed layers which varies between 2.2 and 2.4 Å. In this case the important factor which influences the cation distribution between octahedral interstices is the compensation of electrostatic repulsion between high charged cations in adjacent octahedra. This repulsion may be overcome by formation of metal–metal bonds as they are present in Ru-containing hexagonal perovskites ($BaRuO_3$ (1), $Ba_4Ru_3MO_{12}$ (M = Na, Li) (2), and $Ba_3Ru_2MO_9$ (M = Zn, Ni) (3)). When bonding between B cations is impossible, the repulsion can be diminished by the occupation of octahedral interstices in h-type lamellae by cations with small formal charges ($Ba_4M_3LiO_{12}$ (M = Ta, Nb) (4), $Ba_5W_3Li_2O_{12}$ (5) or by cations and vacancies. The simplest example of a fully ordered distribution of high charged cations and vacancies in the chains of FSO is the $Ba_5Ta_4O_{15}$ crystal structure (6) which is based on a ($hccch$) close packing sequence and contains chains of three face-sharing octahedra. The cation vacancies are located in the central octahedron while the Ta ions are in the others; this leads to the largest distance between Ta^{5+} cations. When part of Ta^{5+} cations are replaced by Ti^{4+} ions the formation of $Ba_{10}Ta_{7.04}Ti_{1.2}O_{30}$ and $Ba_8Ta_4Ti_3O_{24}$ compounds is possible (7). Their structures are based on a 10H $(cchcc)_2$ and a 8H $(cchc)_2$ close-packing, respectively. The reduction of electrostatic repulsion between the two high-charged cations in adjacent octahedra in (chc) lamellae is achieved by the existence of two different types of pairs of FSO. One of them is statistically occupied by 50% Ta and 50% vacancies (□). In the $Ba_{10}Ta_{7.04}Ti_{1.2}O_{30}$ structure the average occupancies of the two types of FSO are very close: (0.5 Ta + 0.5 □) and (0.56 (Ta, Ti) + 0.44 □). This leads to a disordered location of these FSO. In the $Ba_8Ta_4Ti_3O_{24}$ structure the occupancy of the second FSO type (0.875 (Ta, Ti) + 0.125 □) essentially differs from that for the first pair (0.5 Ta + 0.5 □) and FSO pairs are arranged in an ordered manner.

In the present paper we describe the results of the synthesis and the structural investigation of the new hexagonal perovskite-like oxide $Ba_8Ta_6NiO_{24}$ with cation vacancies in the B positions. Its crystal structure is closely related to that of $Ba_8Ta_4Ti_3O_{24}$. The distribution of B cations between octahedral interstices was determined by X-ray powder crystal structure refinement and confirmed by high resolution electron microscopy.

2. EXPERIMENTAL

Samples with nominal composition $Ba_8Ta_{6+0.4x}Ni_{1-x}O_{24}$ ($-0.2 \le x \le 0.2$; $\Delta x = 0.1$) were prepared by a solid state reaction where $BaCO_3$ dried at 400°C, Ta_2O_5, and NiO were used as initial reagents. Stoichiometric mixtures of oxides were ground in an agate mortar under acetone and

0022-4596/96 $18.00

TABLE 1
Crystallographic Data for $Ba_8Ta_6NiO_{24}$

Space group	$P6_3cm$
a, Å	10.07458(6)
c, Å	19.0122(2)
V, Å^3	1671.16(2)
Z	3
2θ range, degrees	7–120
Number of refinable parameters	63
Number of possible reflections	956
R_F, R_P, R_{wP}	0.028, 0.042, 0.056
Texture parameter along 001 axis	0.955(2)

pressed into pellets. The pellets were heated at 1150°C for 24 h. Then they were reground, pressed again, and heated at 1350°C for 40 h. A ''Nabertherm'' furnace was used for the 1150°C heat treatment and a furnace with lanthanum chromite heaters was used for the 1350°C annealing. The synthesis was carried out in Al_2O_3 crucibles in air. All samples were finally furnace cooled.

The phase composition and the lattice parameters of the samples were determined by X-ray powder diffraction using a Guinier FR-552 camera (Cu$K\alpha_1$ radiation, λ = 1.54056 Å; Ge was used as an internal standard). Raw data for crystal structure refinement were collected using the STADI-P powder diffractometer (Cu$K\alpha$ radiation, reflection mode, step 0.02° 2θ, acquisition time 40 sec, scintillation counter). The sample for the crystal structure determination was prepared using about 30 vol% of starch to suppress the strong preferred orientation of the crystallites.

TABLE 2
Positional and Thermal Parameters for $Ba_8Ta_6NiO_{24}$

Atom	Position	x/a	y/b	z/c	B, Å^2
Ba1	2*a*	0	0	0.25	1.12(6)
Ba2	4*b*	1/3	2/3	0.2345(5)	1.12(6)
Ba3	6*c*	0.658(1)	0	0.603(2)	1.12(6)
Ba4	6*c*	0.3087(7)	0	0.880(2)	1.12(6)
Ba5	6*c*	0.334(2)	0	0.490(2)	1.12(6)
Ta1[a]	4*b*	1/3	2/3	0.424(1)	0.59(4)
Ta2[b]	4*b*	1/3	2/3	0.057(1)	0.59(4)
Ta3	2*a*	0	0	0.051(1)	0.59(4)
Ta4	6*c*	0.3321(8)	0	0.678(2)	0.59(4)
Ta5	6*c*	0.6587(8)	0	0.803(2)	0.59(4)
O1	6*c*	0.501(9)	0	0.238(5)	1.0
O2	6*c*	0.190(6)	0.190(6)	0.871(3)	1.0
O3	6*c*	0.145(6)	0.145(6)	0.496(3)	1.0
O4	12*d*	0.653(6)	0.159(4)	0.497(3)	1.0
O5	12*d*	0.334(9)	0.166(9)	0.242(5)	1.0
O6	12*d*	0.688(5)	0.174(5)	0.124(3)	1.0
O7	6*c*	0.156(8)	0.156(8)	0.121(5)	1.0
O8	12*d*	0.490(7)	0.320(4)	0.864(4)	1.0

[a] $-g$ = 0.85Ta.
[b] $-g$ = 0.75 Ni + 0.15 Ta.

TABLE 3
Main Interatomic Distances for $Ba_8Ta_6NiO_{24}$

Ba1–O2 2.99(6) × 3	Ta1–O4 2.18(5) × 3
–O7 2.91(9) × 3	–O8 2.06(6) × 3
–O5 2.92(9) × 6	–Ta2 2.52(4) × 1
Ba2–O1 2.909(2) × 3	Ta2–O4 2.04(5) × 3
–O6 2.71(5) × 3	–O6 2.14(6) × 3
–O5 2.91(11) × 3	–Ta1 2.52(4) × 1
–O8 3.00(6) × 3	
Ba3–O1 3.03(10) × 1	Ta3–O3 1.80(6) × 3
–O6 2.76(4) × 2	–O7 2.06(9) × 3
–O3 2.84(7) × 1	
–O6 3.04(5) × 2	
–O4 2.58(5) × 2	
–O7 3.01(9) × 2	
–O5 3.15(10) × 2	
Ba4–O1 3.31(10) × 1	Ta4–O1 2.03(10) × 1
–O5 3.07(10) × 2	–O5 2.07(10) × 2
–O2 2.72(6) × 2	–O6 1.95(5) × 2
–O8 2.82(4) × 2	–O7 2.08(9) × 1
–O3 2.75(7) × 1	
–O8 3.26(7) × 2	
–O4 2.88(5) × 2	
Ba5–O2 2.68(7) × 1	Ta5–O1 2.03(10) × 1
–O6 3.05(6) × 2	–O2 1.99(7) × 1
–O3 2.92(7) × 2	–O5 2.07(10) × 2
–O7 3.08(10) × 1	–O8 1.99(7) × 2
–O4 2.79(6) × 2	
–O8 2.90(7) × 2	
–O4 3.03(5) × 2	

The crystal structure was refined using the GSAS program package. The Rietveld method with a modified pseudo-Voigt profile function was used for the final refinement. The influence of a preferred orientation along the [001] axis was taken into account by the March–Dollas function. An absorption function was included in the refinement because the surface roughness effect led to remarkable distortions of the intensities in the small angle range and to negative thermal parameters for some atoms. After correction, the thermal parameters of the cations were positive but the thermal parameters of the oxygen atoms still had a tendency to become slightly negative. They were fixed to be equal to 1.0 Å^2 for the final refinement, which did not change either the values of the reliability factors or the atomic coordinates. The thermal parameters for the Ba atoms and the B cations were combined in two separate blocks to overcome strong correlations and were refined in an isotropic approximation.

Samples for high resolution electron microscopy were obtained after crushing parts of the pellet and dispersing the powder on a copper grid, dipped in a soft glue. The material was investigated in a Jeol 4000EX microscope with a point resolution of 1.8 Å.

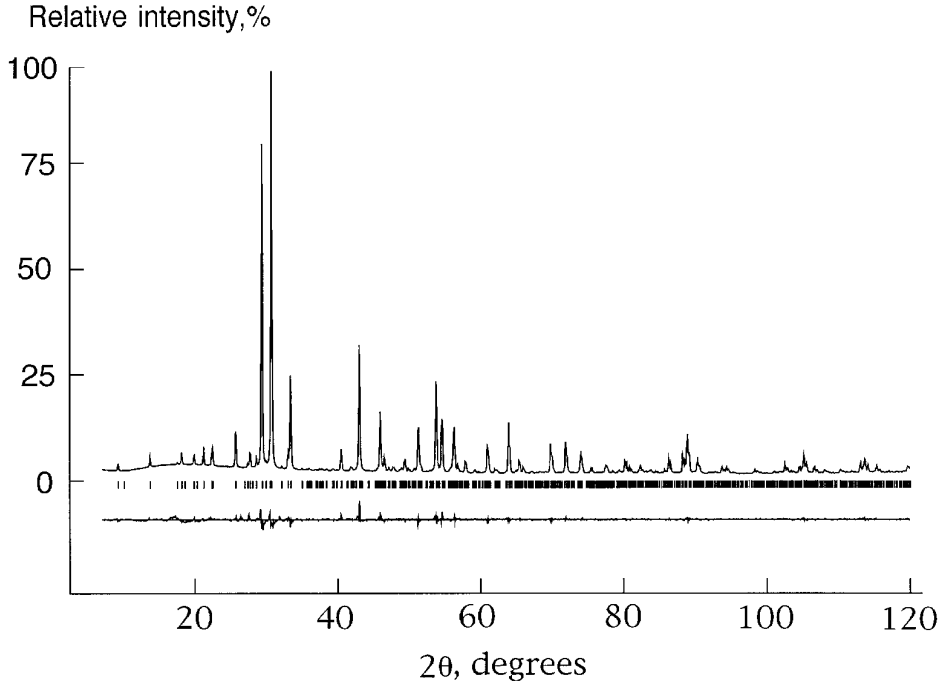

FIG. 1. Experimental, calculated, and difference X-ray pattern for $Ba_8Ta_6NiO_{24}$.

3. RESULTS AND DISCUSSION

3.1. X-Ray Measurements

The X-ray diffraction pattern revealed a single phase sample for the nominal composition $Ba_8Ta_6NiO_{24}$ and it was indexed on a hexagonal lattice with cell parameters $a = 10.0738(1)$ Å, $c = 19.0105(1)$ Å. The X-ray diffraction pattern of the $Ba_8Ta_6NiO_{24}$ compound is very similar to that of $Ba_8Ta_4Ti_3O_{24}$, therefore we propose the same space symmetry and similar atomic coordinates for both structures. Since the reflections $h0l$ for l odd are systematically absent on the X-ray pattern, we suggest the centrosymmetric $P6_3/mcm$ space group or the corresponding noncentrosymmetric $P6_3cm$ one.

The starting model was refined with the $P6_3/mcm$ space group. The refinement led to unreasonable values of the reliability factors ($R_F = 0.086$) and a high value of the thermal parameter (2.7 Å^2) for the Ta atom in the (0, 0, z) position. Changing the $P6_3/mcm$ space group to the noncentrosymmetric $P6_3cm$ allowed one to the split atomic positions in the centers of the FSO and to perform a separate refinement. The further refinement was thus carried out in the $P6_3cm$ space group. The refinement of the corresponding occupancies showed that all cation positions in the center of corner-shared octahedra (6c) are completely occupied by Ta atoms. A refinement of the occupancies for the two (0, 0, z) positions (2a) revealed that the first ($z = 0.05$) is completely filled by tantalum atoms, while the second ($z = 0.43$) remains empty.

The average occupation (1 Ta + 0.75 Ni + 0.25 □) of the remaining FSO pair situated at (1/3, 2/3, z) can be deduced from the nominal composition of the compound $Ba_8Ta_6NiO_{24}$ ($Z = 3$). The electron densities in both positions were estimated by the refinement (with fixed thermal parameters) of its occupancies assuming a filling by only Ta atoms. The approximate values of $g = 0.855(9)$ and $g = 0.33(1)$ for the positions with $z = 0.42$ and $z = 0.056$, respectively, were obtained after this procedure. When 1 Ta atom was placed into the first position and 0.75 Ni atoms were placed into the second, the following values for the reliability factors were obtained: $R_F = 0.032$, $R_P = 0.043$, $R_{wP} = 0.057$. However, the best approximation was achieved by using (0.85 Ta + 0.15 □) and (0.15 Ta + 0.75 Ni + 0.1 □) occupations for the (1/3, 2/3, 0.42) and (1/3, 2/3, 0.056) positions. It should be noted that the variation of the occupancy factors with the remaining electron densities for both positions did not change significantly the interatomic distances and the thermal parameters. Finally, the following values of reliability factors were obtained: $R_F = 0.028$, $R_P = 0.042$, $R_{wP} = 0.056$. The crystallographic data for $Ba_8Ta_6NiO_{24}$ are summarized in Table 1. Positional and thermal parameters and main interatomic distances for $Ba_8Ta_6NiO_{24}$ are listed in Tables 2 and 3, respectively. Experimental, calculated, and difference X-ray patterns are shown in Fig. 1.

Figure 2 illustrates the relationship between the basic vectors and the superstructure vectors as well as the location of the different FSO pairs in the unit cell of the Ba_8

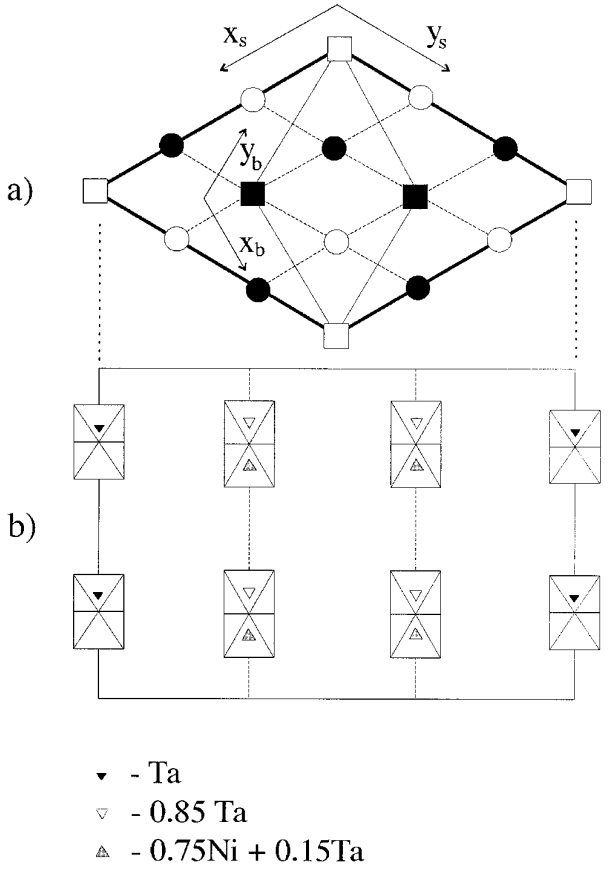

FIG. 2. Schematic representation of the $Ba_8Ta_6NiO_{24}$ crystal structure. (a) [001] projection; X_b and Y_b represent the axes of the basic cell, while X_s and Y_s are the axes for the superstructure unit cell. (b) [110] projection; empty squares correspond to the position of the first type of FSO in a 00z position; filled squares represent FSO of the second type. Filled and empty circles represent the 1/3, 2/3, z and 2/3, 1/3, z positions in the basic cell, respectively.

Ta_6NiO_{24} structure. The location of the cation vacancy in only one octahedron of the FSO pair (marked by empty squares) results in a shift of the Ta atom from the center of the neighboring octahedron toward the common triangular face formed by the O3 atoms. This leads to a decrease of the Ta3–O3 distance to 1.80 Å while the Ta3–O7 distance is 2.06 Å; the Ta3 atoms have a distorted octahedral arrangement. The second FSO pairs are located inside the unit cell along the (1/3, 2/3, z) and the (2/3, 1/3, z) axis (marked by filled squares). Obviously, the observed metal–metal separation in this case is an average one between the Ta–Ni and the Ta–□ distance. This distance of 2.52 Å is significantly larger than the average thickness of a BaO_3 layer (2.38 Å) which can be calculated by dividing the c parameter by the number of close-packed layers in the unit cell. However, an increase in the metal–metal distance does not lead to an elongation of the Ta1–O4 and the Ta2–O4 bond lengths and the coordination polyhedra for both cations are close to an ideal octahedron. It should be noted that the metal–metal separation (2.52 Å) in the second type of FSO pairs of the $Ba_8Ta_6NiO_{24}$ structure is appreciably shorter than the corresponding distance in the $Ba_8Ta_4Ti_3O_{24}$ structure (2.64 Å). This is due to a smaller electrostatic repulsion between the Ta^{5+} and Ni^{2+} cations in comparison with the repulsion between two Ti^{4+}. The Ta cations in the corner-sharing octahedra have practically an undistorted octahedral oxygen environment. The Ba atoms have slightly distorted 12-coordinated polyhedra.

Both $Ba_8Ta_6NiO_{24}$ and $Ba_8Ta_4Ti_3O_{24}$ structures are closely related and based on the same construction principles. Obviously, the ''*chc*'' lamellae where both interstices in the FSO are occupied by Ta^{5+} cations should be unstable

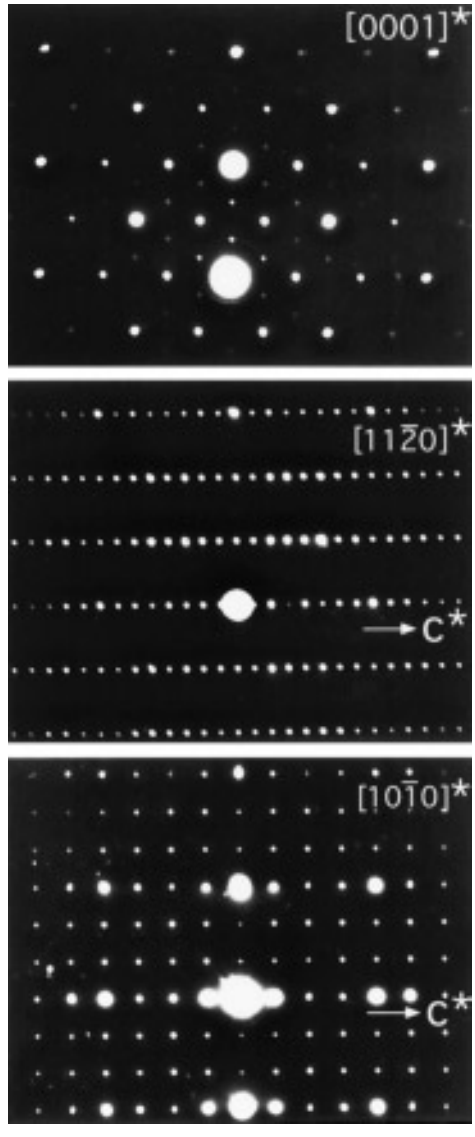

FIG. 3. [0001]*, [11$\bar{2}$0]*, and [10$\bar{1}$0]* electron diffraction patterns of $Ba_8Ta_6NiO_{24}$; these patterns are in agreement with the structure determined by X-ray diffraction.

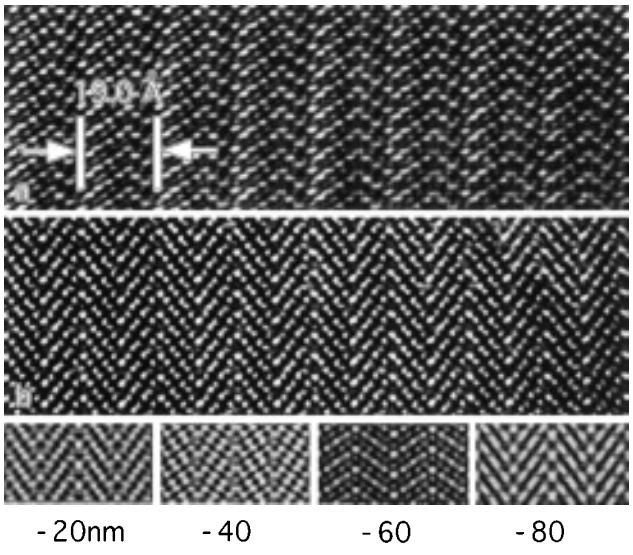

FIG. 4. (a, b) Experimental HREM images of $Ba_8Ta_6NiO_{24}$ along the $[10\bar{1}0]$ zone for two different defocus values, close to −60 nm (a) and close to −20 nm (b). A series of calculated images based on the atom positions of Table 2 is shown in the bottom figure (thickness 40 Å, focus values ranging between −20 and −80 nm).

since the metal–metal separation is very short and the electrostatic repulsion is very large. The exchange of Ti^{4+} cations in the $Ba_8Ta_4Ti_3O_{24}$ structure for Ni^{2+} cations leads to an increase in the Ta^{5+} content to keep the electrostatic balance and, as a consequence, a change in the occupation of the octahedral interstices. In contrast to the $Ba_8Ta_4Ti_3O_{24}$ structure, the $Ba_8Ta_6NiO_{24}$ structure induces further ordering of cations and vacancies in the FSO pairs. One of the possible reasons for such ordering may be found in a stronger difference between the charges of the *B* cations (Ni^{2+} and Ta^{5+}) in comparison with the Ti–Ta-containing compound. The ordered location of the tantalum atoms and vacancies in two neighboring FSO leads to the appearance of much stronger superstructure reflections than for the $Ba_8Ta_4Ti_3O_{24}$ compound and they can be easily detected in the X-ray powder pattern.

$Ba_8Ta_4Ti_3O_{24}$ oxide has a wide range of homogeneity when Ti atoms are substituted by Ta atoms and a $Ba_8Ta_{4+0.8x}Ti_{3-x}O_{24}$ solid solution is formed. We assume that the substitution takes place in the second type of FSO statistically occupied by Ta and Ti cations and vacancies. We could only detect a small homogeneity range for the $Ba_8Ta_{6+0.4x}Ni_{1-x}O_{24}$ solid solution for positive x as well as for negative x values. The lattice parameters change from a = 10.0674(6) Å, c = 19.002(2) Å for x = 0.2 to a = 10.0735(8) Å, c = 19.023(2) Å for x = −0.2. Assuming that substitution takes place only on the second FSO pairs, the narrow homogeneity range for this solid solution may be explained by a practically complete ordering of Ta, Ni cations and vacancies in this type of FSO.

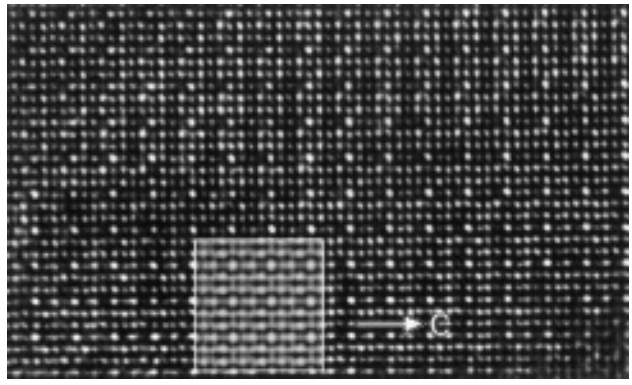

FIG. 5. HREM of $Ba_8Ta_6NiO_{24}$ along the $[11\bar{2}0]$ zone. A calculated image (thickness 40 Å, defocus −300 Å), based on the atom positions of Table 2 is shown as an inset.

3.2. Electron Diffraction and Electron Microscopy

The most prominent electron diffraction patterns of $Ba_8Ta_6NiO_{24}$, [0001]*, $[11\bar{2}0]$*, and $[10\bar{1}0]$*, are produced in Fig. 3; they confirm the structure determined by X-ray diffraction, although some of the extinction conditions formulated before are violated here because of double diffraction. This is, e.g., the case for the 000*l* reflections, where the reflections with $l = 2n + 1$ should be extinct. This is the case in the $[10\bar{1}0]$ section, but not in the $[11\bar{2}0]$ section where these reflections occur by double diffraction from $hh\bar{0}l$ rows.

The diffraction patterns are very similar to those reported for the $Ba_8Ta_4Ti_3O_{24}$ compound (7), however in the $[10\bar{1}0]$ section the superstructure spots are more pronounced (compare to Fig. 1c in (7), indicating a better ordering of cations and vacancies in the face-sharing octahedra (FSO) pairs.

High resolution images of the $Ba_8Ta_6NiO_{24}$ structure have been obtained along the most relevant zones, such as $[10\bar{1}0]$ and $[11\bar{2}0]$; they are shown in Figs. 4 and 5, respectively. Along the $[10\bar{1}0]$ zone, the structure is viewed along the close packed Ba–O–Ba rows and the image directly reveals the sub-unit cell twinned structure. The Ba–O–Ba–O columns are imaged as the brightest dots, while the less intense dots in between the bright dots image the *B* cations in the octahedral interstices. This interpretation is in agreement with the calculated images, taking as input the structure described above, as deduced from X-rays and using the microscope parameters for different thicknesses and focus values (see bottom line of Fig. 4 or inset of Fig. 5). The ordered location of the tantalum atoms and vacancies in the FSO is directly visualized in the $[10\bar{1}0]$ section; the intensity of bright dots on both sides of the (vertical) mirror plane of the structure is no longer equal and translates the unequivalent filling of the octahedra.

The $[11\bar{2}0]$ section, where the equivalent FSO are

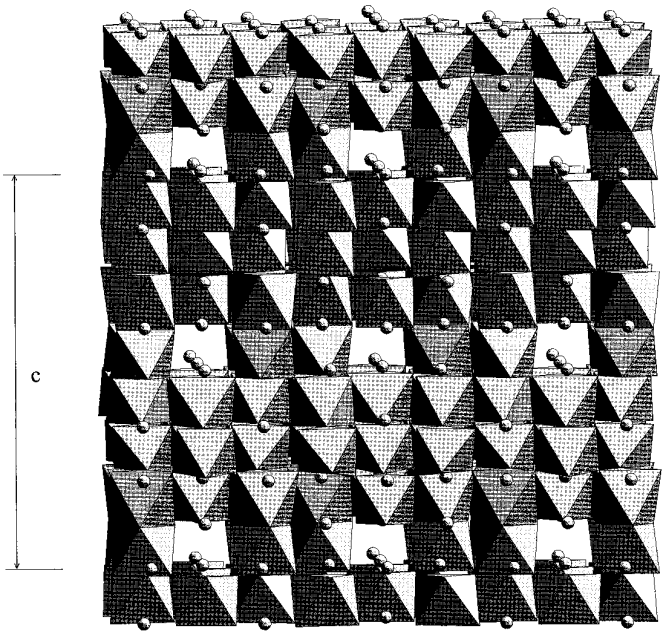

FIG. 6. Projected structure of $Ba_8Ta_6NiO_{24}$ along $[11\bar{2}0]$, where the positions of the empty FSO are clearly in agreement with the observed superstructure in Fig. 5.

aligned and form columns, allows the position and configuration of the empty FSO in the structure to be imaged very nicely (see the projected image of Fig. 6). For the $Ba_8Ta_4Ti_3O_{24}$ structure this superstructure, and therefore the ordering, was much less defined. The present interpretation is confirmed by image simulations based on the X-ray structure; a calculated image for a thickness of 40 Å and a focus value of −300 Å is shown as an inset in Fig. 5.

Deviations from perfection, e.g., stacking errors or twinning dislocations, are only occasionally met. Such defects however have been described in detail in (7) for the $Ba_8Ta_4Ti_3O_{24}$ structure; for $Ba_8Ta_6NiO_{24}$ these defects are very similar and therefore we refer to (7) for a detailed discussion.

ACKNOWLEDGMENTS

The authors are grateful to O. Lebedev and S. Amelinckx for their interest and scientific discussions. This work was supported by the Russian Science Foundation and an individual fellowship from the International Soros Science Education Program (a471-h).

REFERENCES

1. P. C. Donohue, L. Katz, and R. Ward, *Inorg. Chem.* **43,** 306 (1965).
2. P. D. Battle, S. H. Kim, and A. V. Powell, *J. Solid State Chem.* **101,** 161 (1980).
3. P. Lightfoot and P. D. Battle, *J. Solid State Chem.* **89,** 174 (1990).
4. B. M. Collins, A. J. Jacobson, and B. E. F. Fender, *J. Solid State Chem.* **10,** 29 (1974).
5. A. J. Jacobson, B. M. Collins, and B. E. F. Fender, *Acta Crystallogr. Sect. B* **30,** 816 (1974).
6. J. Shannon and L. Katz, *Acta Crystallogr. Sect. B* **26,** 102 (1970).
7. R. V. Shpanchenko, L. Nistor, G. Van Tendeloo, J. Van Landuyt, S. Amelinckx, A. M. Abakumov, E. V. Antipov, and L. M. Kovba, *J. Solid State Chem.* **114,** 560 (1995).